ELSEVIER

Contents lists available at ScienceDirect

## **Energy Storage Materials**

journal homepage: www.elsevier.com/locate/ensm





# Carbon nanotubes grafted conductive polymer constructs robust multi-scale conductive pathways for high-performance anodes

Lu Wang <sup>a</sup>, Yan Zhao <sup>a,b,\*</sup>, Hao Zhang <sup>a</sup>, Haoliang Wang <sup>a</sup>, Chuanxi Chen <sup>a</sup>, Yuxiang Huang <sup>a</sup>, Haoyu Xue <sup>a</sup>, Yumeng Lan <sup>a</sup>, Fen Qiao <sup>b</sup>, Junfeng Wang <sup>b,c</sup>, Zirui Lou <sup>a,\*\*</sup>, Feng Pan <sup>a,\*\*</sup>

- <sup>a</sup> School of Advanced Materials, Peking University Shenzhen Graduate School, Shenzhen, 518055, China
- <sup>b</sup> School of Energy and Power Engineering, Jiangsu University, Zhenjiang, 212013, China
- <sup>c</sup> School of Energy and Power Engineering, Chongqing University, Chongqing, 400030, China

#### ARTICLE INFO

#### Keywords: Silicon-based anode Electron transport networks Carbon nanotubes Conductive binder Solid-electrolyte interphase

#### ABSTRACT

As the representative high-performance anode, the performance of silicon-based anode in high-energy lithium-ion batteries is hindered by significant volumetric fluctuations and poor conductivity. Carbon nanotubes (CNTs) have emerged as pivotal conductive additives and structural stabilizers in silicon-based electrodes. However, the insulation of commercial binders and their limited interaction with CNTs prevent the CNTs from performing their intended roles, particularly in commercial electrodes with high anode material content. To address this, the study introduces a novel conductive binder (PCNT) by grafting conductive polyfluorene onto the surface of CNTs. The long/short-range electron transport channels intertwine to form a dense, multi-scale conductive network, which endows the binder with remarkable conductivity and efficient electron transfer at the CNTs interface, significantly reducing voltage polarization in graphite/SiO<sub>x</sub> electrodes and enhancing rate performance. Even with an ultra-low binder content (5 wt % without other additives), the constructed robust framework effectively suppresses electrode expansion and internal void cracking, which helps decelerate the aging process of solid-electrolyte interphase (SEI). Thus, it maintains the integrity of the electronic percolation network, improving the cycling stability of the electrodes. The effective synergy between conductivity, adhesiveness, and mechanical properties offers new insights into the application of CNTs and conductive polymers in silicon-based electrodes.

#### 1. Introduction

Stricter requirements from the industry for power batteries and consumer batteries are gradually driving the iteration of various key materials in lithium-ion batteries (LIBs), especially the low theoretical capacity (372 mAh  $g^{-1}$ ) of commercial graphite anode limits the overall energy density [1–3]. As a representative of high theoretical specific capacity and cost-effective anode,  $SiO_X$  (0 < x < 2) materials are gradually being utilized and capturing a certain share of the market [2–5]. In conventional silicon-based electrodes (Fig. 1a), conductive carbon black serves as an additive, forming an electron transport network through continuous contact. However, as the mechanical properties of commercial binders (e.g., sodium carboxymethyl cellulose/styrene butadiene rubber (CMC/SBR), polyacrylic acid (PAA)) [6–8] are not sufficient to inhibit the expansion of silica-based anodes, the electronic percolation network is gradually disrupted by particle expansion and the

thickening of the solid-electrolyte interphase (SEI) at the interfaces [4,5, 9]. This disruption leads to electrochemical inactivation of  $\mathrm{SiO}_{x}$  particles, thus limiting the large-scale industrial application of silicon-based materials.

Carbon nanotubes (CNTs) (Fig. 1b) are added as highly conductive additives to real-world silicon-based electrodes. They not only functions as a rigid skeleton to enhance the structural strength of the electrode in combination with the binder, but also provides a long-range electron transport channel to maintain the conductive skeleton of the electrodes [10,11]. Liu et al. constructed a resilient and robust conductive network in silicon-based electrodes by utilizing the amidation reaction of amino-functionalized CNTs with PAA, alongside the multiple hydrogen-bonding interactions between tannic acid and PAA/carboxyl nitrile rubber, thereby enhancing the cycling performance of micron-sized silicon/SiO $_{\rm x}$  electrodes [12]. Cao and colleagues have intricately woven a resilient electron transport network by leveraging

E-mail addresses: zhaoyan@ujs.edu.cn (Y. Zhao), zrlou@pku.edu.cn (Z. Lou), panfeng@pkusz.edu.cn (F. Pan).

<sup>\*</sup> Corresponding author at: School of Energy and Power Engineering, Jiangsu University, Zhenjiang, 212013, China.

<sup>\*\*</sup> Corresponding authors.

carboxylated CNTs and PAA, along with 6-amino-1-hexanol, through hydrogen bonding, ionic interactions, and covalent bonds, thereby achieving a high areal capacity for high-mass-loading Si/C electrodes [13]. Although these studies have attempted to address this issue by enhancing the mechanical properties of adhesive systems, achieving promising results, the failure of the electron percolation network is only mitigated and is still inevitable due to the insulation properties of conventional polymers.

The conductive polymers, which can serve as artificial electron transport networks at particle interfaces and provide high mechanical strength, are being used as binders in silicon-based anodes [6,7]. In the previous works, [14–18]. silica-based conductive binders (polyfluorene) integrate cohesiveness, mechanical properties, and conductivity to expand the electron transport channels between particles beyond the traditional electron permeation network dominated by conductive carbon. However, the conductivity of conductive polymers in general is always limited, and the addition of highly conductive agents are needed to provide an "electron highway" for conductive networks. As previously

mentioned, CNTs can offer fast electron transport channels and facilitate electron conduction over scales in comparison with conductive polymers. When used in conjunction, a more comprehensive spatial network of electron transport can be constructed within the electrode. Therefore, combining conductive binders with CNTs presents a potentially optimal approach for stabilizing the electron transport network and spatial structure in silicon-based anodes, a novel finding yet to be reported.

In order to construct robust multi-scale electron transport channels, this study develops a novel composite conductive binder (Fig. 1c) by grafting conductive polyfluorene (PF) chains, which act as short-range electron transport channels, onto CNTs that serve as long-range ones. The intertwining of these long/short-range pathways forms a continuous three-dimensional conductive network. Compared to the blending method, the CNTs grafted conductive binder (PCNT) system improves the dispersion of CNTs in aqueous solvents and establishes a quasi-reinforced concrete structure through covalent bonding between CNTs and polymer chains. It boosts the mechanical strength and electron connectivity of the conductive network. Despite an extremely low

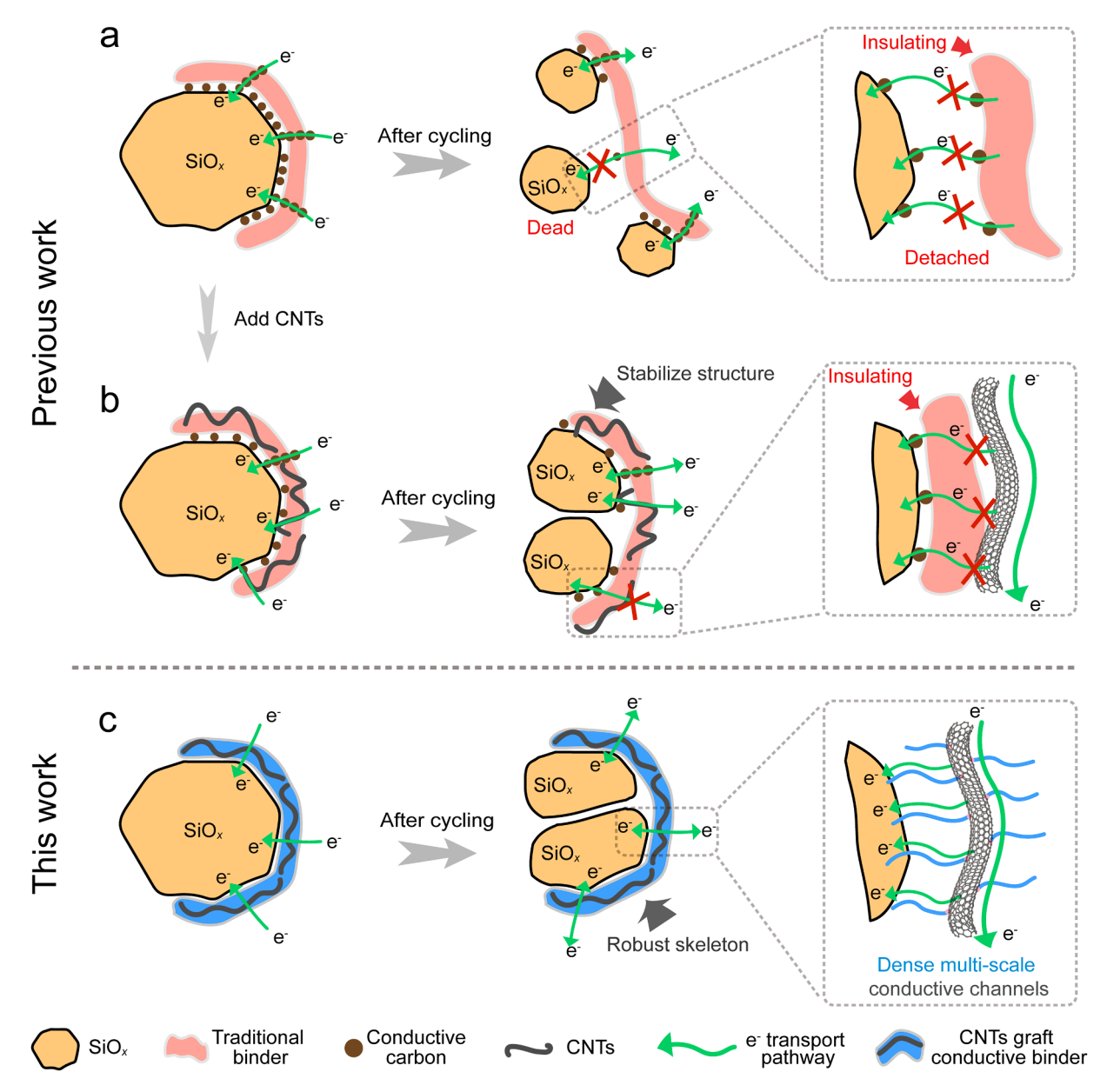


Fig. 1. Schematic illustration of (a) conductive network constructed by conventional binder and conductive carbon (b) conductive network constructed by conventional binder, conductive carbon and CNTs (c) long-range and short-range electron transport channels constructed by CNTs grafted conductive polymers (PCNT) in the electrode.

binder content (5 wt %), the constructed dense conductive network effectively facilitated a marked depolarization effect in the silicon-based electrode, releasing more capacity. The robust binder framework restricted electrode expansion, minimized internal void, and significantly slowed the aging of the SEI at particle interfaces, thereby enhancing the cycle life of the commercial graphite/SiO $_{\rm X}$  (Gr/SiO $_{\rm X}$ ) electrode. Additionally, the synergistic effect between the binder and well-constructed SEI establishes a stable network for the infiltration of both electron and lithium-ion (Li $^{+}$ ), resulting in exceptional rate performance of the electrode.

#### 2. Results and discussion

#### 2.1. Design principles of multi-scale conductive interwoven networks

To graft conductive polyfluorene chains onto the surface of CNTs, aryl bromides were introduced to carboxylated carbon nanotubes (CNTCOOH) through amidation reactions, yielding CNT-Br (Fig. S1). Fourier transform infrared (FTIR) spectroscopy (Fig. S2) confirmed the modification, revealing distinct amide group peaks on the surfaces of CNT-NH $_2$  and CNT-Br, characterized by stretching vibrations of C=O and C=N, as well as bending vibrations of C=N-H [19–22]. Similarly, in X-ray photoelectron spectroscopy (XPS) (Fig. S3), the C-Br and O=C=NH

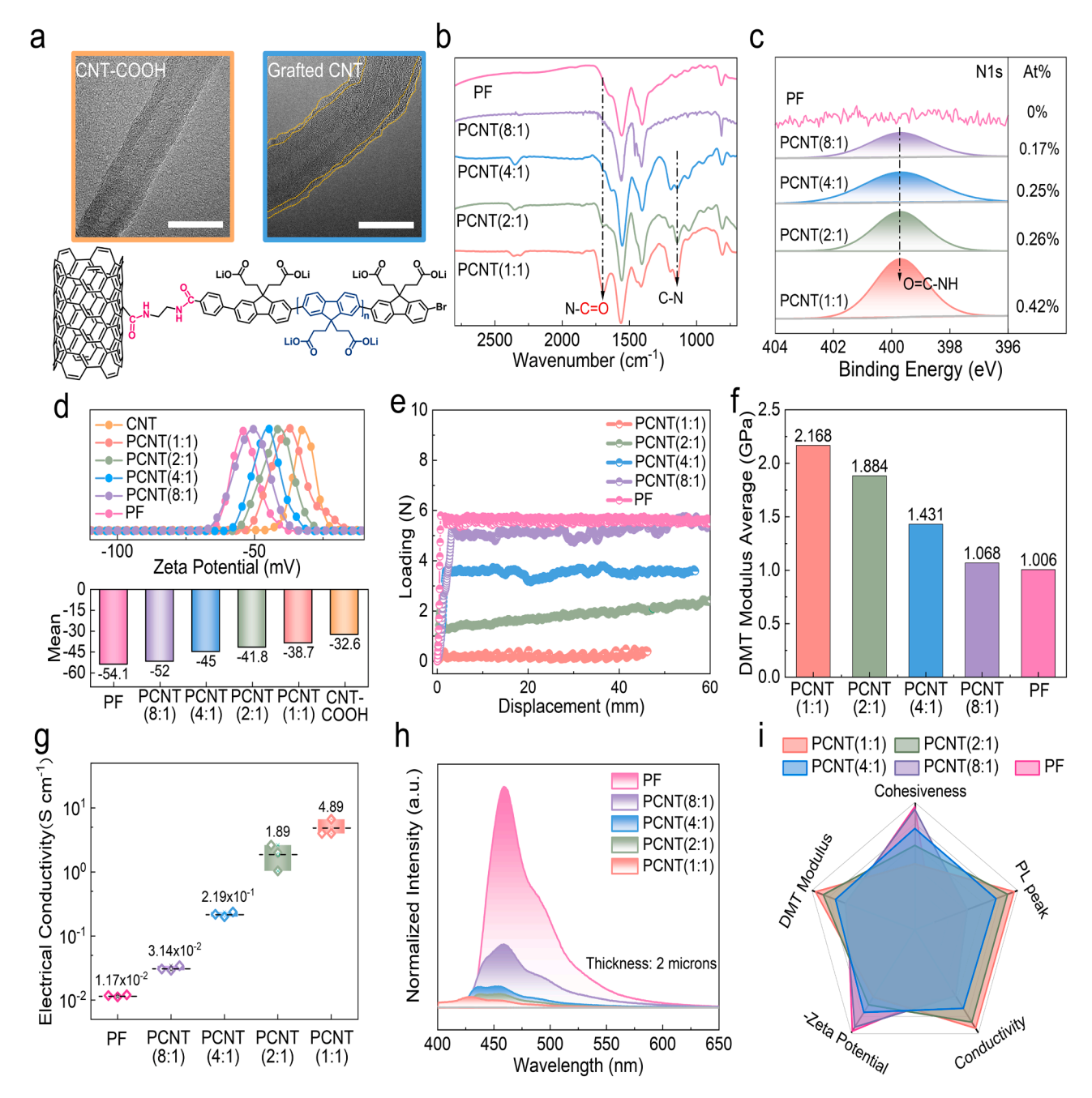


Fig. 2. Synthesis and screening of the ideal ratio of PCNT binders. (a) TEM images of CNT-COOH and grafted CNTs. The scale bar of the images represents 20 nm. (b) FTIR spectra of the pure conductive binder (PF) and PCNT. (c) High-resolution XPS N 1 s spectra of the PF and PCNT. (d) The zeta potential of the CNT-COOH, the PF and PCNT. (e) The 180° peeling profiles between different films and copper foils. (f) DMT modulus average of the PCNT membranes. (g) Electronic conductivity of the membranes. (h) Photoluminescence (PL) spectra of the membranes (thickness: 2 μm). (i) Ideal CNTs weight ratio is selected based on electronic conductivity, cohesiveness, Zeta potential, PL peak intensity and DMT modulus.

peaks were attributed to the successful introduction of aryl bromides [20,22]. After etching 60 s (Figs. S4 and S5), the intensity of the characteristic peaks significantly diminished, and the proportion of nitrogen atoms decreased from  $1\,\%$  to  $0.2\,\%$ , indicating that the grafting reaction sites are concentrated on the outer walls.

The PCNT binders were prepared through a Suzuki coupling reaction shown in Fig. S6. In order to investigate the effect of CNT content, the modified CNT-Br was incorporated into the polymerization system of conductive polymer (polyfluorene, PF) at various weight ratios (PF/CNT-Br = 8:1, 4:1, 2:1, 1:1), yielding CNTs grafted conductive polymer binders at different weight ratios (PCNT (8:1), PCNT (4:1), PCNT (2:1), PCNT (1:1)) (Table S1). Compared to CNT-COOH, the TEM images (Fig. 2a) of the PCNT binder reveal a continuous amorphous organic layer coating the tube walls, directly indicating the uniform grafting of conductive polymers onto the CNTs surface. As the CNTs weight ratio increases, more polymer chains graft onto the active surface sites, corresponding to the increasing intensity of the N-C=O and C-N stretching vibration peaks in the FTIR spectra (Fig. 2b). Furthermore, the enhanced peak intensity of amide groups in the XPS (Fig. 2c) further corroborates this finding.

The basic properties of the PCNT binders are explored to select the optimal ratio of PF to CNTs. Firstly, CNT-COOH exhibits poor dispersibility in water, with the lowest absolute value of zeta potential (Fig. 2d). Introducing water-soluble conductive polymers onto the surface of CNTs enhanced their dispersibility in aqueous solutions. As the polymer content increases, the absolute value of the zeta potential of PCNT binder rises, leading to improved stability of the CNTs in the solution system. This increased dispersibility stability could prevent aggregation of CNTs, ensuring the formation of a uniform structural framework and efficient electron transport pathways within the electrodes. The resistance of the PCNT binders to shear forces increases with the higher PF ratio, indicating improved adhesion. It can be attributed to increased content of carboxylate side chains of the polymers grafted onto CNTs (Fig. 2e). The abundant carboxyl groups may engage in hydrogen bonding interactions or form ester bonds with the hydroxyl groups on the surface of SiO<sub>x</sub> particles. During lithiation, the strong interactions prevent the active particles from detaching from the conductive network, thereby maintaining the electrochemical activity of

Increasing the CNTs content in the binder system enhances the Derjaguin-Muller-Toporov (DMT) modulus (Fig. 2f) of PCNT, resulting in a more robust framework to better resist the expansion of SiO<sub>x</sub> particles. However, the AFM mapping images (Fig. S7) show that during the molding process of the binder film, carbon nanotubes of PCNT (1:1) and PCNT (2:1) tend to agglomerate, exhibiting rigid regions of high modulus that are prone to stress concentrations during lithiation and delithiation, damaging the electrode structure. Polyfluorene, with its continuous conjugated backbone, demonstrates a conductivity of  $1.17 \times 10^{-2}$  S cm<sup>-1</sup> (Fig. 2 g and S8) significantly higher than commercial binders such as CMC/SBR ( $2.51 \times 10^{-11}$  S cm<sup>-1</sup>). Upon grafting highly conductive CNTs, the macroscopic conductivity of the binder can be improved by 1 to 2 orders of magnitude, and the conductivity of PCNT binder (PCNT (1:1)) can reach 4.89 S cm<sup>-1</sup>. To explore the impact of CNTs content on electron transfer between CNTs and the conductive polymer, photoluminescence (PL) spectra were measured for various binder films (Fig. 2h). The pure polyfluorene polymer films absorb photons to produce excitons. When excitons return to the ground state within polyfluorene units, photons are emitted, producing distinct characteristic PL peaks in the spectrum (425-575 nm). As the CNTs content increases, more conjugated segments contact the tube walls, result in sufficient intermolecular exciton transport and dissociation, eventually manifest non-radiative transition fluorescence quenching [23,24]. This finding is evidenced by the gradual reduction in the intensity of the PL peaks. Considering the impact of CNTs weight proportion on dispersion, adhesion, overall conductivity, and charge transfer between CNTs and the polymer (Fig. 2i), the balance in

performance is achieved when the CNTs content is around 20 %. Therefore, PCNT (4:1) is selected as the representative binder for subsequent electrode fabrication.

#### 2.2. The advantages of the multi-scale conductive network

In order to investigate the specific advantages of PCNT binder, pure conductive polymer (PF) was mixed with CNTs in various ratios to obtain PF/CNTs blended binder systems, namely BPCNT (8:1), BPCNT (4:1), BPCNT (2:1) and BPCNT (1:1). Firstly, the dispersion of different binder systems in deionized water was assessed through zeta potential testing at various levels of CNTs addition (Fig. 3a-c and S9). The PCNT binders exhibited a narrow, single Zeta potential peak, indicating that the bonding of water-soluble polymer chains to the CNTs surface enhanced their dispersion in deionized water. In contrast, the zeta potential of the blended BPCNT binder presented multiple peaks. Moreover, the intensity of the peaks with lower absolute potential values grew stronger as the amount of CNTs increased, suggesting the challenge in achieving a stable and uniform binder dispersion solution.

The effect of grafted conductive polymers on electron transport in PCNT binder was investigated by four-probe test. When the CNTs content was 1/9, the conductivity of the grafted binder PCNT (8:1) improved, while the conductivity of the blended binder BPCNT (8:1) remained similar to that of polyfluorene (Fig. S10). In BPCNT (Fig. 3d), owing to  $\pi$ - $\pi$  stacking interactions, the conjugated main chains of some polymers draw near to the surface of the CNTs. Their anionic side chains extend outward, resulting in the repulsion of the remaining polymers. As the anionic side chains push each other away, continuous electron transport is consequently impeded. In PCNT, the main chains of conductive polymer are anchored to the walls of nanotubes, where they mutually repel each other, thus forming spread planetary-like molecular-level electron transport channels. When the CNTs weight fraction reached 20 wt % (Fig. 3e), more polymers were grafted onto the CNTs, resulting in a conductivity improvement by an order of magnitude in PCNT (4:1). However, the increase in conductivity in BPCNT (4:1) was not as substantial. When the CNTs content reaches 50 wt %, the longrange conductive pathways established by the CNTs interconnect to become the primary conduits for electron transport. This transition results in the conductivity of PCNT and BPCNT binders becoming approximately equal. The previous section has already demonstrated that the proportion of CNTs in the binder system should not be excessively high. Therefore, enhancing the interaction between conductive polymers and CNTs, while maintaining a moderate CNTs content, aids in constructing a more continuous conductive network, thereby improving macroscopic conductivity overall.

PL spectroscopy was conducted to investigate the difference in electron transfer capacity between CNTs and PF in the two binder systems (Fig. 3f and S11). As the CNTs content increased, the PL peak intensity of the PCNT binder was lower than that of the BPCNT binder. This finding indicates that the conductive polymers grafted onto the CNTs surface increased the contact with each other, facilitating smoother local electron transfer between the two components. This is clearly illustrated by the TEM images (Fig. S12). The surface of the CNTs in the PCNT binder is covered with a layer of amorphous conductive polymer, and almost no polymer is observed on the surface of the CNTs of the BPCNT binder. This may derive from the lack of interaction between polymer and CNTs in BPCNT, the polymer was washed away after the sample preparation using the solution dispersion-drip method. Moreover, when the CNTs content was relatively low, the PL peak intensity of PCNT (8:1) exceeded that of BPCNT (8:1). At this ratio (Fig. S13), there are more free conductive polymer segments that are farther away from the grafted segments as well as the CNTs surface due to repulsion between anionic groups, which limits the contact between the CNTs and free PF chains, thus hindering local electron transfer. Therefore, when increasing the polymer content in PCNT binders to improve its adhesion and dispersion, it is worth noting that the free

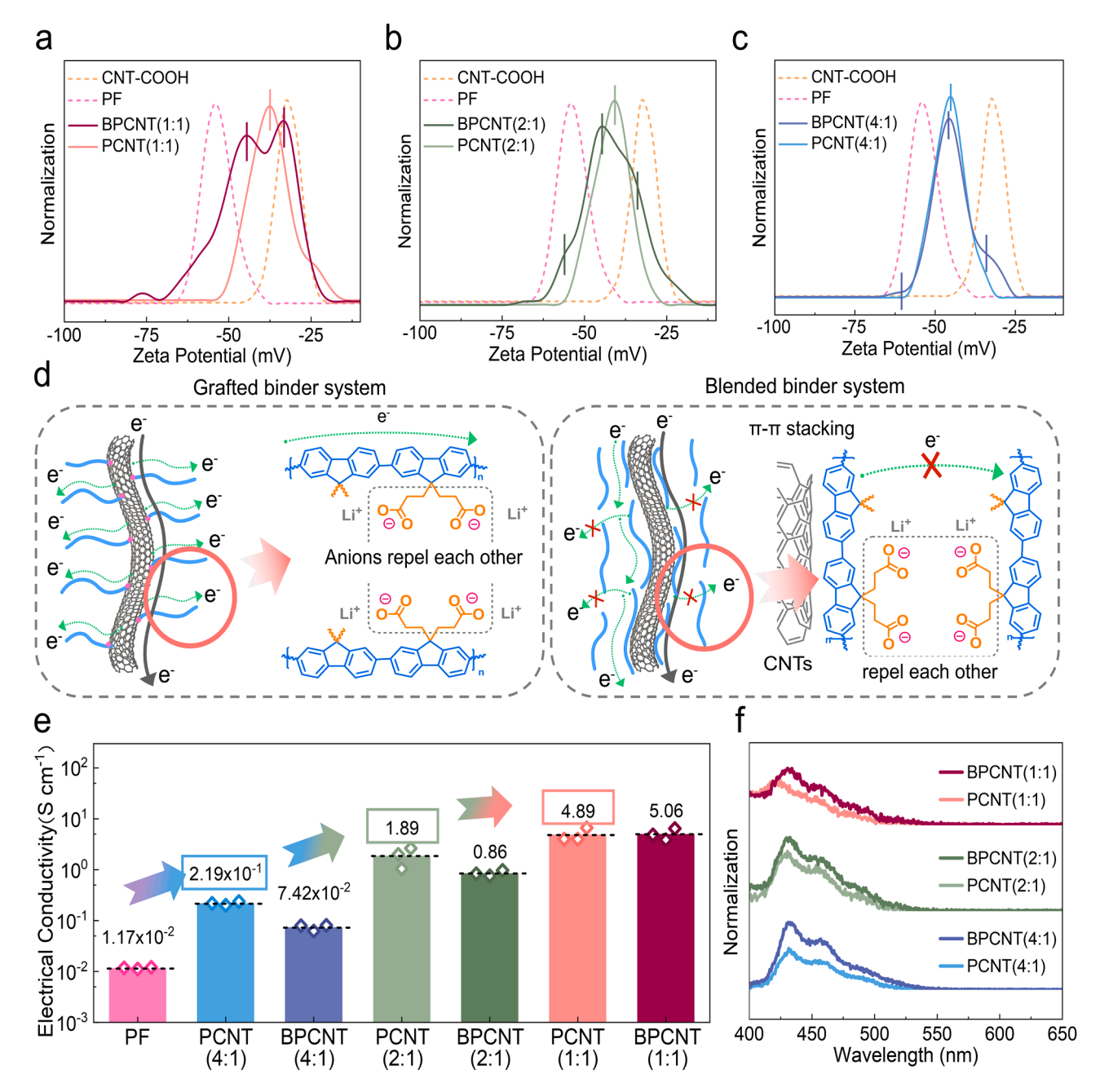


Fig. 3. Compared to blending conductive polymers with CNTs, the PCNT has more advantages. Zeta potential distribution curves of (a) PCNT (1:1) and BPCNT (1:1), (b) PCNT (2:1) and BPCNT (2:1), (c) PCNT (4:1) and BPCNT (4:1). (d) Differences in conductive pathways of grafted binder systems and blended binder systems at the CNTs interface. (e) The electronic conductivity of grafted or ungrafted CNTs conductive binder membranes. (f) The PL spectra of grafted versus ungrafted CNTs conductive binders (thickness:  $5 \mu m$ ).

polymer segments will cause limited improvement in macroscopic conductivity and limit the ability of efficient electron transfer between local CNTs and conjugated segments. In other words, optimal macroscopic and electron transport efficiency of the binder may be achieved when all polyfluorene segments in the system are grafted onto CNTs surface.

The in-situ Raman spectra and finite element simulations were conducted to assess the protective function of the grafted polymer layer on the CNTs (Fig. S14-S15 and Table S2) between CNTs and active particles. During the lithiation process, the downshift (from 1592 cm $^{-1}$  to 1550c m $^{-1}$ ) of the G band represents the tensile strain of the CNTs in the BPCNT (4:1) electrode. Further deep lithiation leads to the emergence of high-strain peak (1445 cm $^{-1}$ ), as well as  $sp^3$  peaks representing new defects and silicon band peak exposed by expansion. The result

shows that the grafted polymer layer in PCNT binders served as a buffer between the CNTs and the particle during the expansion process. It enabled stress dissipation and maintained the integrity of the conductive network. However, the polymer layer in BPCNT binders fails to fully cover the surface of the CNTs, resulting in localized stress concentrations where the CNTs contact with the particles. This phenomenon leads to particle pulverization and damage to the CNTs. Therefore, the PCNT binder integrates the macroscopic electron transport channel (CNTs) (Fig. S16) with the microscopic electron transport channel (polyfluorene). This integration yields a robust and interconnected conductive network, exhibiting remarkable conductivity, dispersibility and mechanical properties.

#### 2.3. Improved electrochemical performance of Gr/SiO<sub>x</sub> electrodes

The electrochemical performance of the  ${\rm Gr/SiO}_x$  (Fig. S17) (5wt % binder/additive) ||Li half-cells was evaluated using galvanostatic charge-discharge tests. Firstly, the initial cycle voltage profile (Fig. 4a) shows that the PCNT (4:1) electrode exhibits the lowest polarization among three conductive binders, attributed to the dense long/short-range electron transport channels constructed by the CNTs intertwined with conductive polymers. Following the in-situ electrochemical impedance spectroscopy (EIS) analysis presented in Fig. 4b, it is evident that incorporating CNTs as long-range electron transport pathways significantly reduces the impedance of the  ${\rm Gr/SiO}_x$  electrode and the PCNT (4:1) electrode exhibits the lowest impedance after the initial

lithium intercalation. This phenomenon can be attributed to improved conductivity of the N-type doped polyfluorene and the hierarchical conductive network by PCNT. Consequently, even with minimal addition of PCNT binder, an effective depolarization network is built within the silicon-based anode, leading to an increased capacity at the same potential.

The electrochemical performance of CMC/SBR electrodes is also evaluated using  ${\rm Gr/SiO}_X$  coin cells. Three additional types of  ${\rm Gr/SiO}_X$  electrodes are fabricated as control samples using conventional CMC/SBR binders: the electrode with Super P (SP) alone (CMC/SBR/SP), the electrode with only CNTs (CMC/SBR/CNTs), and the electrode with both CNTs and SP (CMC/SBR/SP/CNTs). Long-term cycling performance (Fig. S18) shows that the CMC/SBR/CNTs electrode exhibits a

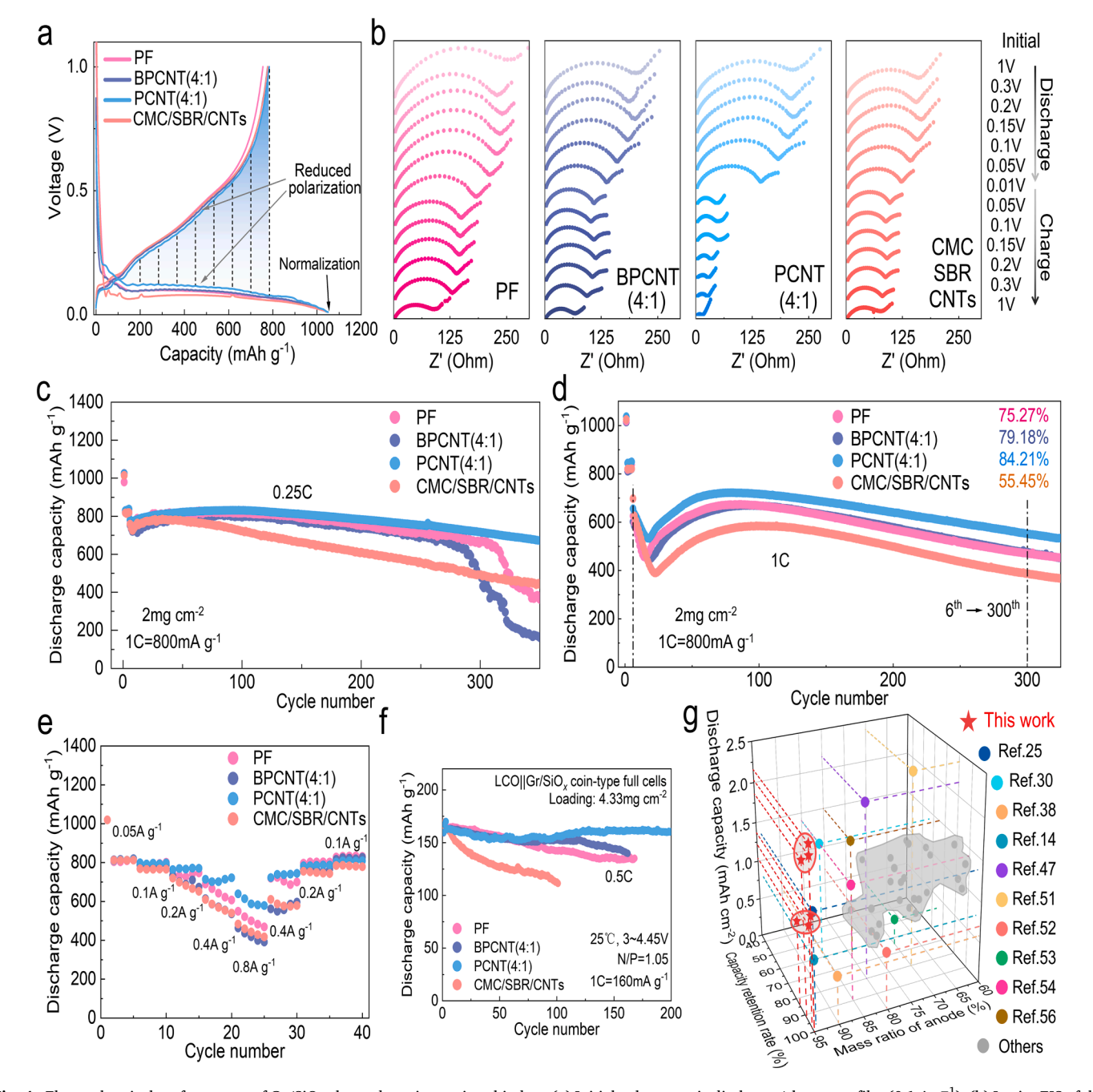


Fig. 4. Electrochemical performances of  $Gr/SiO_x$  electrodes using various binders. (a) Initial galvanostatic discharge/charge profiles (0.1 A  $g^{-1}$ ). (b) In-situ EIS of the electrodes at initial cycle (half-cell). Cycling performance of the electrodes at a current density of (c) 0.2 A  $g^{-1}$  and (d) 0.8 A  $g^{-1}$ . (e) Rate performance of the electrodes. (f) Cycling performance of  $LCO||Gr/SiO_x$  coin-type full cells. (g) Electrochemical performance comparison between our work and previously reported typical binders for  $SiO_x$  electrodes [14,25–58].

specific capacity of 429 mAh  $g^{-1}$  after 250 cycles, outperforming the other two. Although incorporating CNTs as long-range electron transport channels reduces the polarization of the CMC/SBR/SP electrode and releases more reversible capacity (Fig. S19a), this enhancement is limited. In the CMC/SBR/CNTs electrode (Fig. S19b), the absence of conductive carbon (SP) leads to a capacity limitation of the graphite material due to increased electrode polarization. In contrast, the internal structural stability facilitates the release of capacity in the  $SiO_x$  material. Therefore, for silicon-based anodes, it is only by constructing a robust, dense conductive network within the electrode that its full potential can be realized. Therefore, grafting the conductive polymer, which serves as short-range electron transport channels, onto the surface of CNTs not only provides molecular-level conductive pathways between particles but also collaborates with CNTs to construct the stable structural framework.

The long-term cycling curves (Fig. 4c) reveal that the PCNT (4:1) (5 wt %) electrode exhibits a specific capacity of 672 mAh g<sup>-1</sup> after 350 cycles at 0.25 C, indicating a notable capacity retention rate of 86.0 %. However, the PF electrode (Fig. S20a), due to the limited mechanical strength, fails to suppress electrode cracking. Consequently, this failure results in continuous side reactions with the electrolyte until the electrolyte is completely consumed, causing a sharp decline in electrochemical performance after 300 cycles. Interestingly, the BPCNT electrode experiences worse cycling performance. The lack of interaction between CNTs and the conductive polymer allows the CNTs to pierce through the SEI, [59]. leading to direct exposure to the electrolyte and triggering more vigorous reactions. In contrast, the PCNT (4:1) binder effectively binds polyfluorene and CNTs, interlinking them to form a robust structural framework for the electrode. The structure effectively prevents direct contact of the electrolyte with CNTs, avoiding subsequent electrolyte decomposition and the formation of a thick interfacial layer. Thus, the electrode using PCNT (4:1) exhibits the highest capacity retention of 84.2 %, corresponding to a specific capacity of 552 mAh g-1 after 300 cycles at 1 C (Fig. 4d). In addition, the  $SiO_x$  electrode using PCNT (4:1) binder also shows excellent cycling performance (Fig. S20b). The potential profiles (Fig. S21) of different cells after 300 cycles clearly illustrate the significant advantage of the PCNT (4:1) electrode in minimizing overpotential. This result demonstrates that the intertwined conductive network of long-range and short-range connections plays a significant role in lowering voltage polarization.

The coulombic efficiency curves of four electrodes are depicted in Fig. S22. The coulombic efficiency of the PCNT (4:1) electrode reached 99.3 % after 7 cycles and remained stable above 99.8 % in subsequent cycles without any fluctuations, suggesting the formation of a stable SEI. In contrast, the curve of the BPCNT (4:1) electrode exhibits fluctuations during cycling. This could be attributed to the repeated puncturing of the SEI caused by rigid CNTs during the expansion of silicon-based particles. This finding is further demonstrated by the EIS (Fig. S23). BPCNT (4:1) electrode exhibited an increase in the resistance of the SEI layer (R<sub>SEI</sub>) during cycling, while the PCNT (4:1) electrode maintains the lowest R<sub>SEI</sub>. The incorporation of conductive binder significantly reduces the charge transfer resistance (Rct) of the electrodes, which could be attributed to their molecular-level contact with active materials. Grafting it onto the surface of CNTs helps stabilize the bulk-structure of the electrode, ensuring the continuity and integrity of the electron transport network, thereby maintaining Rct at a lower value. The fourprobe conductivity test (Fig. S24) of the cycled electrodes also demonstrates that the introduction of conductive polymers ensures the effective electron percolation network during cycling, thereby stabilizing the capacity release of the Gr/SiO<sub>x</sub> electrodes. The superior electronic conductivity of the binder network in the PCNT (4:1) electrode further elevates its electrochemical performance. In addition, temperaturedependent EIS was used to explore the lithium-ion diffusion energy barrier of the SEI layer on the anode surface. According to the Arrhenius equation, the calculated activation energy of lithium-ion diffusion

through SEI and electron transfer activation energy (Fig. S25) indicate that the binder network constructed by PCNT (4:1) maintains the low lithium-ion diffusion energy barrier through the SEI layer on the particle surface. Therefore, the PCNT (4:1) not only constructs an excellent electron percolation network, but also prevents lithium-ion diffusion blockage at the interface. This stabilizes interfacial charge transfer on the silicon-based particles, thereby enabling the electrode to exhibit exceptional rate performance (Fig. 4e and S26).

LCO||Gr/SiO $_x$  coin-type full cells were also assembled to further evaluate the electrochemical performance of the PCNT electrode. As expected, the full cell exhibits 98.6 % capacity retention within 200 cycles at 0.5 C, outperforming other cells in performance (Fig. 4f). In short, although the PCNT binder accounts for only 5 wt % of the total weight in Gr/SiO $_x$  electrodes, compared with previously reported typical binders (Fig. 4 g and Table S3), the constructed interwoven multi-scale conductive network still enables stable long-term cycling and excellent rate performance of electrodes with high anode material content. It is attributed to the thorough preservation of the bulk-structure and the interphase of the electrodes.

#### 2.4. Reinforced structural stability of cycled electrodes

To reveal the reinforcing effect of the concrete structural framework constructed by PCNT on the bulk-structure of the Gr/SiO<sub>x</sub> electrodes, insitu expansion test (Fig. 5a-c) was conducted in the coin cell. During the initial lithiation, the PF electrode exhibits the initial expansion rate of 104 %. The addition of CNTs effectively restrained the electrode's swelling, reducing the expansion rate of the BPCNT (4:1) electrode to 87 %. The PCNT (4:1) electrode leveraged CNTs to crosslink low molecular weight conductive polymer, maximizing CNTs as reinforcing structures to enhance stability, ultimately limiting the expansion rate to 80 %. Moreover, the swelling of the PCNT (4:1) electrode remained stable throughout subsequent cycles, whereas the expansion curves of the other two electrodes continued to rise. It is worth mentioning that the PF electrode, which lacks long-range structural components, exhibited varying degrees of local fracturing, as indicated by the irregular fluctuations in the expansion curve. In the CMC/SBR binder system (Fig. S27), the initial expansion rate of the CMC/SBR/SP electrode reaches as high as 135 %, while the addition of CNTs reduce the electrode's expansion rate. Moreover, the CMC/SBR/CNTs electrode exhibits higher reversible expansion during subsequent cycles, further demonstrating that carbon nanotubes, in addition to facilitating electron transport, also play a crucial role as structural components in siliconbased electrodes.

The PCNT binder, on the one hand, utilizes the abundant carboxyl groups of the conductive polyfluorene side chains to interact strongly with the hydroxyl groups on the surface of SiO<sub>x</sub> particles, providing localized adhesive strength (Fig. S28). On the other hand, it leverages the unique shape and outstanding mechanical properties of CNTs to interconnect these local adhesive networks, thereby constructing a robust rebar-like structure that limits the electrode's expansion, akin to reinforced concrete. The top-view SEM image (Fig. S29) of the PCNT (4:1) electrode after 200 cycles demonstrates the preservation of surface integrity and continuity. The cross-sectional SEM images (Fig. 5d-f and S30) more clearly reveal the structural advantages of the PCNT binder. In the traditional CMC/SBR system, the incorporation of carbon nanotubes significantly prevents the formation of large continuous void during expansion. Similarly, this enhancement in structural stability is also reflected in the controlled void expansion of the BPCNT (4:1) electrode compared to the PF electrode. For the PCNT (4:1) electrode, despite 200 cycles at 1C, the cross-sectional SEM image shows only minimal porosity. It is attributed to the robust, quasi-reinforced concrete structure, which plays a crucial role in limiting electrode cracking. Understandably, it also reduces the continuous contact between anode particles and the electrolyte, directly influencing the formation of a stable interfacial layer.

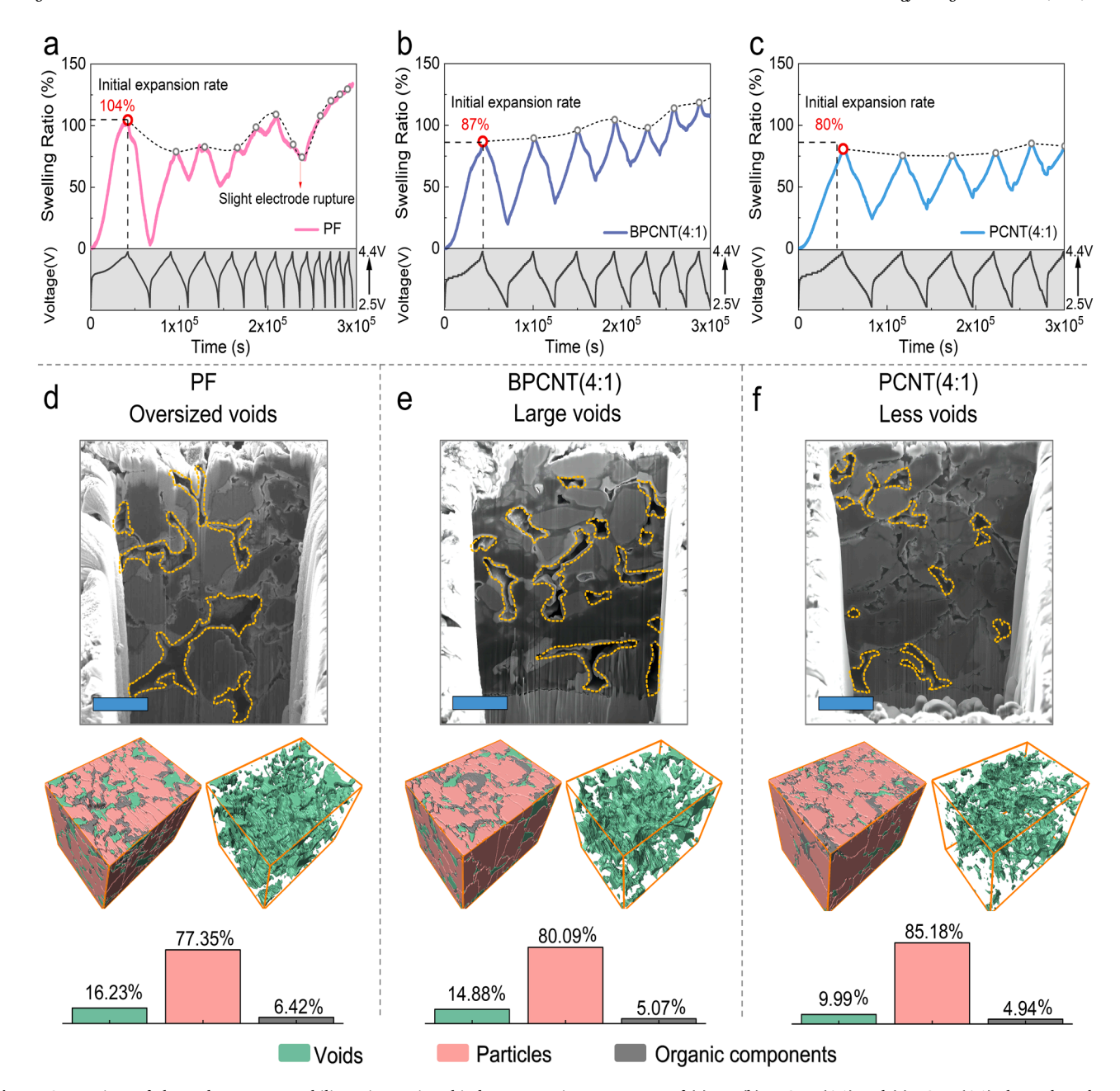
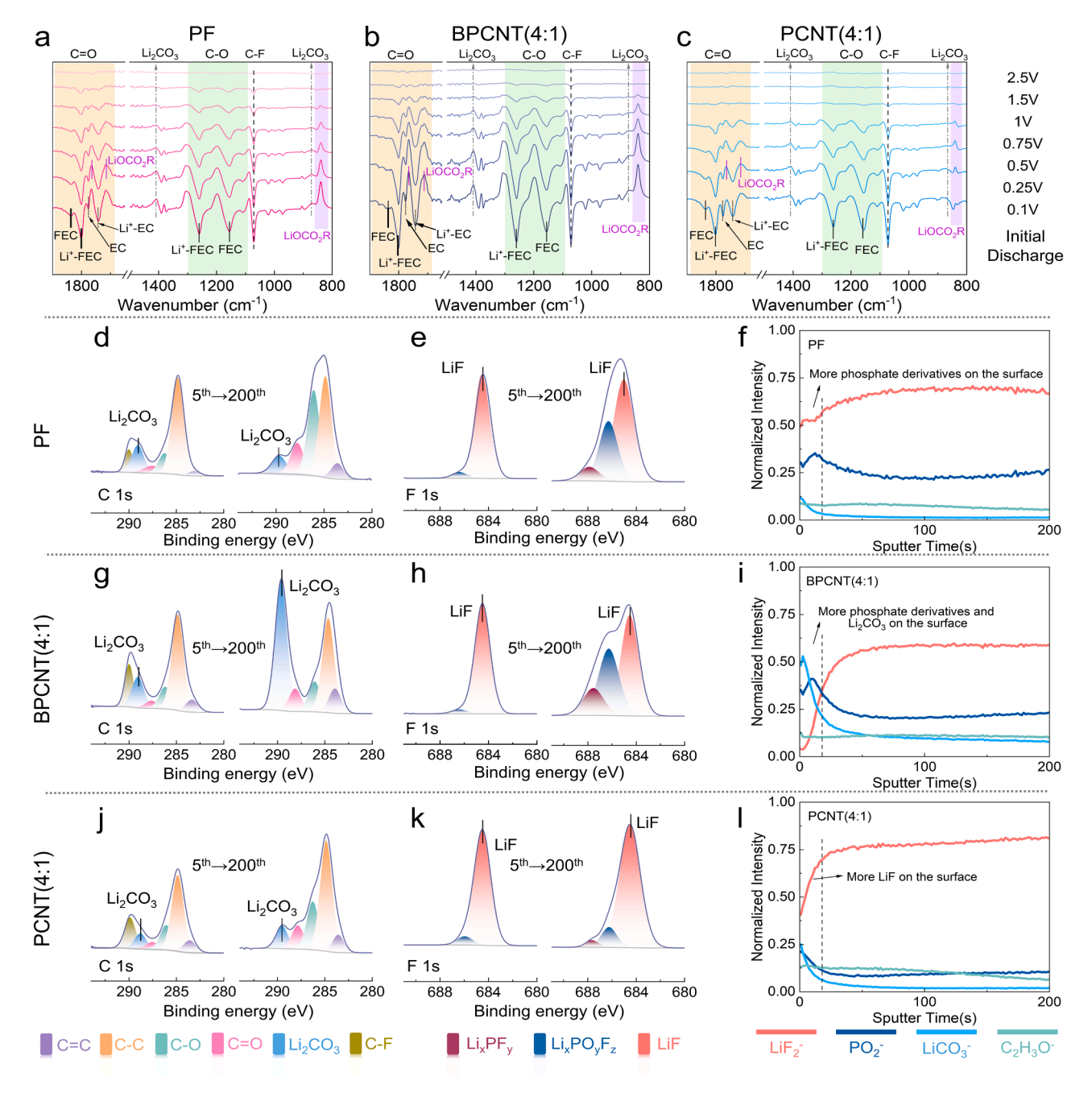


Fig. 5. Comparison of electrode structure stability using various binders. Expansion rate curves of (a) PF, (b) BPCNT (4:1) and (c) PCNT (4:1) electrodes. The FIB-SEM test is used to obtain the cross-sectional SEM and 3D reconstruction images of the (d) PF, (e) BPCNT (4:1) and (f) PCNT (4:1) electrodes.

This finding is further corroborated by the focused ion beam and scanning electron microscopy (FIB-SEM) technology, [9], which reliably confirm these results and offer a comparative analysis of the differences in component content within the electrodes. Reconstruction of a series of SEM images with a step size of 50 nm reveals the three-dimensional structure of the components near the electrode surface (Fig. 5d-f, and S31-33). After 200 cycles, the PF electrode exhibited a bulk porosity of 16.23 %, while the porosity of the BPCNT (4:1) electrode decreased to 14.88 %. In contrast, the porosity of the PCNT (4:1) electrode was confined to 9.99 %, and the pulverization of internal anode particles was also effectively suppressed. Consequently, the contact between the electrolyte and anode particles decreased, promoting the formation of stable SEI at the interface. In comparison, the repeated fracture and regrowth of the interfacial layer in the other two electrodes led to an increase in the proportion of organic components. Therefore, the exceptional electrochemical performance of silicon-based electrodes is inseparable from the structural stability of the electrodes, which is directly linked to the stability of SEI.

#### 2.5. Enhanced interphasial stability of the electrodes

The binder, as the main component of the interfacial phase on the surface of the anode particles, directly influences the derivation of the SEI during electrochemical processes. In-situ FTIR spectra (Fig. 6a-c) were used to analyze the evolution of SEI at the interface of the anode particles during the initial galvanostatic discharge process. The FTIR signal measured at 2.5 V is used as a baseline, while the downward peak detected in-situ indicates the depletion of electrolyte components near the electrode surface. When the voltage decreases from 2.5 V to 0.1 V, the presence of characteristic peaks regarding floroethylene carbonate (FEC) and ethylene carbonate (EC) indicates that they are consumed at the electrode surface [60–62]. Compared with the PCNT (4:1)



**Fig. 6.** The impact of various binders on SEI stability. In-situ FTIR spectra of (a) PF, (b) BPCNT (4:1) and (c) PCNT (4:1) electrodes during initial galvanostatic discharge process (from 2.5 V to 0.1 V). High-resolution XPS C 1 s (d, g, j) and F 1 s (e, h, k) spectra of different electrodes after 5 and 200 cycles. TOF-SIMS depth profiles for PF, BPCNT (4:1) and PCNT (4:1) electrodes (f, i, l) of LiF<sub>2</sub>, PO<sub>2</sub>, LiCO<sub>3</sub> and C<sub>2</sub>H<sub>3</sub>O<sup>-</sup> fragments.

electrodes, PF and BPCNT (4:1) electrodes have stronger signals representing FEC (1835 cm $^{-1}$ ), Li $^+$ –FEC (1800 cm $^{-1}$ , 1153 cm $^{-1}$ ), EC (1776 cm $^{-1}$ ) and Li $^+$ –EC (1742 cm $^{-1}$ , 1257 cm $^{-1}$ ) on the surface indicating more FEC and EC decomposition, and the lithium carbonate (Li $_2$ CO $_3$ ) and organic carbonate components (ROCO $_2$ Li) mainly decomposed from EC were generated [63,64]. The PCNT (4:1) electrode surface mainly undergoes FEC decomposition, and there are few carbonate components, which is related to the construction of the protection of particles by the constructed robust binder structural framework.

XPS and TOF-SIMS measurements (Fig. 6d-1 and S34–35) were employed to further investigate the evolution of SEI on various electrodes after cycling. After five cycles at 0.1C, the surface of anode particles was enriched with LiF derived from the decomposition of FEC and lithium hexafluorophosphate (LiPF<sub>6</sub>) [65]. The LiF-rich SEI layer not

only facilitates lithium-ion transport at the interface as well as passivates the particle interface but also collaborates with the binder, leveraging its high modulus to constrain the expansion of  $\mathrm{SiO}_X$  particles and maintain interphasial charge transfer [60,65–67]. However, the XPS Li 1 s spectrum reveals that the surfaces of the PF and BPCNT (4:1) electrodes contain more decomposition products (Li<sub>2</sub>CO<sub>3</sub>/ROCO<sub>2</sub>Li) of EC, which was consistent with the in-situ FTIR spectra results of the Gr/SiO<sub>X</sub> electrodes during initial discharge. For the PF electrodes, it is due to the fact that the conductive polymer itself has a relatively low molecular weight and is unable to resist the expansion of silicon-based particles, so that the electrolyte is constantly in contact with the surface of the  $\mathrm{SiO}_X$  particles. After mixing CNTs directly into the electrodes, the lack of interaction between the CNTs and the conductive polymer causes the rigid CNTs to puncture the SEI and further contact it with the electrolyte

during swelling.

After 200 cycles at 1C, the PF electrode shows repeated growth of the interfacial layer due to bulk structural cracking, and the LiF component of the initial SEI is diluted by the decomposition products of LiPF<sub>6</sub> (Li<sub>x</sub>PO<sub>v</sub>F<sub>z</sub>, Li<sub>x</sub>PF<sub>v</sub>) and EC (Li<sub>2</sub>CO<sub>3</sub>, ROCO<sub>2</sub>Li) (Fig. 6e), which is also demonstrated by the results presented by the TOF-SIMS depth profiles (Fig. 6f). Therefore, the electrolyte enters the internal void of the electrode, allowing it to carry out continuous side reactions at the particle interface, which leads to the depletion of the electrolyte with the increase of cycle time, directly causing a sudden drop in electrode performance (Fig. 4c). The TEM image (Fig. S36) of the corresponding particle surface shows a thick SEI layer. The continuous increase in lithium carbonate and lithium salt derivatives (Fig. 6h and i) on the surface of the anode particles in the BPCNT (4:1) electrode further reflects that the direct addition of CNTs, which lack interaction with the binder system, is insufficient to meet the demands of high-performance electrodes with a high proportion of silicon-based materials. Even though the high-modulus SEI was initially constructed, it could not prevent the persistent contact between the rigid carbon nanotubes and the electrolyte (Fig. S37), likewise leading to complete electrolyte depletion. For the PCNT (4:1) electrode, the PCNT binder bonds the CNTs with polyfluorene, with polymer chains tightly adhering to the surface of SiO<sub>x</sub>, anchoring the carbon nanotubes firmly to the surface of the anode particles. This forms a reinforced quasi-reinforced concrete structure within the electrode. PCNT (4:1) collaborates with a significant amount of LiF (Fig. 6k and l) at the electrode surface to establish a

stable charge transfer interphase, preventing the carbon nanotubes from piercing the SEI and reacting continuously with the electrolyte (Fig. S38). Galvanostatic intermittent titration (GITT) tests demonstrate that the PCNT (4:1) electrode has a higher Li<sup>+</sup> diffusion coefficient (Fig. S39) after 100 cycles, which can only be contributed by the stable interphasial charge transfer of anode particles.

Briefly, in Gr/SiO<sub>r</sub> electrodes with ultra-low binder contents (Fig. 7), the traditional conductive binders, due to their inherently low molecular weight, fail to provide the necessary mechanical properties to accommodate the expansion and contraction of the electrode during lithiation and delithiation cycles. It leads to a disruption of long-range electron transport and facilitates the ingress of additional electrolyte into the voids, where side reactions occur. After the direct incorporation of CNTs, these one-dimensional, high-strength structural elements enhance the structural stability of the electrode, significantly reducing its expansion. However, due to the lack of strong interactions between the CNTs and the conductive polyfluorene segments, the CNTs struggle to return to their original positions adjacent to the silicon particles after each volumetric change cycle. Consequently, the previously continuous long-range and short-range electron transport channels are disrupted. The PCNT binder incorporate conductive polymer segments that facilitate short-range electron transport with CNTs that enable long-range electron conduction, thereby constructing an interconnected network (Fig. 7). Concurrently, it forms a robust quasi-reinforced concrete structure, which aids in maintaining the integrity of the conductive network and achieving a remarkable synergy between conductivity and

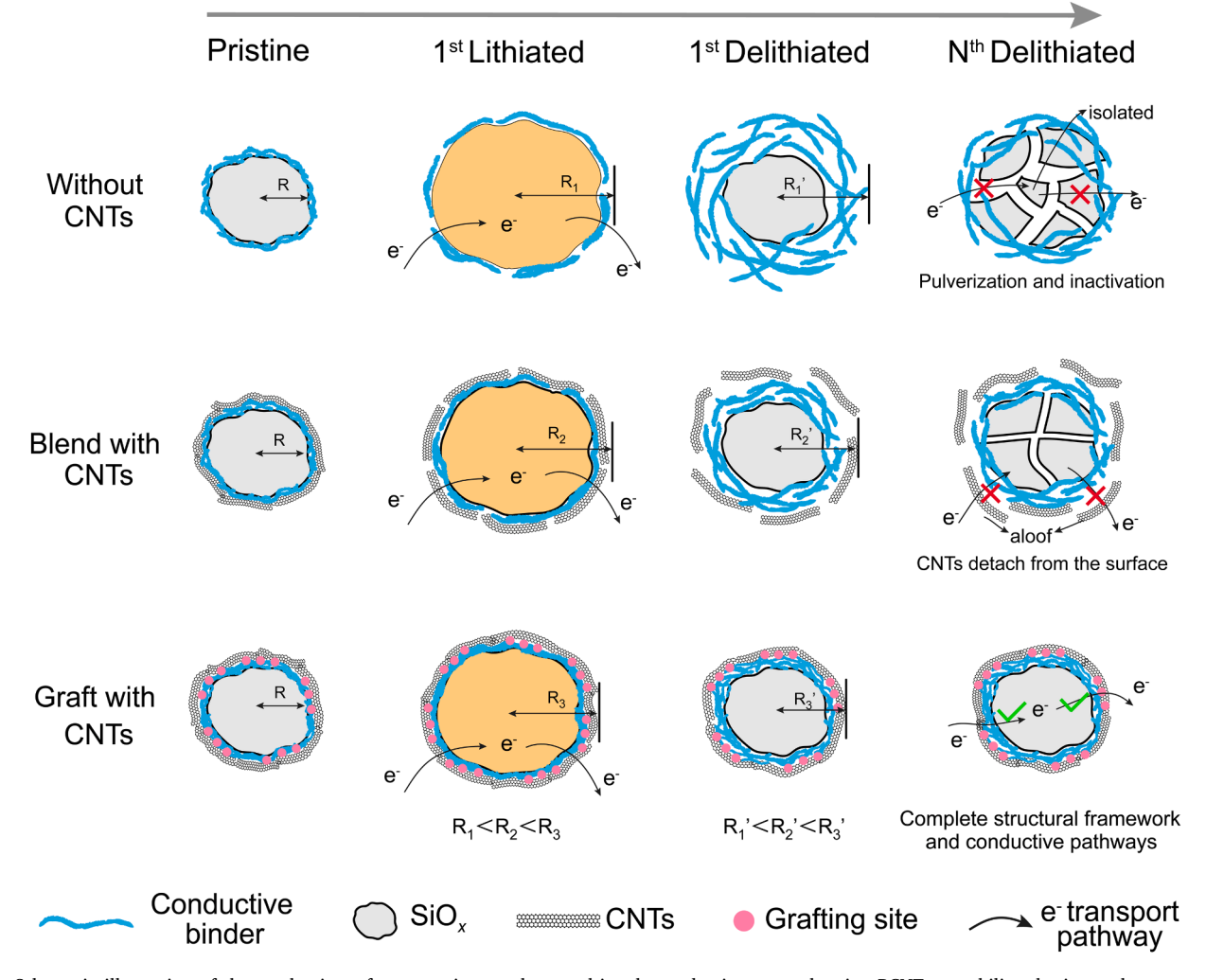


Fig. 7. Schematic illustration of the mechanism of constructing a robust multi-scale conductive network using PCNT to stabilize the internal structure of the electrodes and SEI layer of particles.

mechanical strength. The electron transport network, characterized by remarkable structural stability, effectively constrains the volumetric fluctuations and void expansion of  ${\rm Gr/SiO}_x$  electrodes during charge-discharge cycles. Moreover, the PCNT binders suppresses the acupuncture effect (Fig. S38) of rigid carbon nanotubes on SEI, prevents the side reaction of continuous contact between CNTs and electrolyte, and alleviates the aging of the solid-electrolyte interface at the particle interface, thereby enabling  ${\rm Gr/SiO}_x$  electrodes to attain exceptional electrochemical performance.

#### 3. Conclusion

In summary, the novel polymer-grafted carbon nanotube conductive binder (PCNT) fully leverages the exceptional electrical conductivity and mechanical properties of carbon nanotubes, forming a quasireinforced concrete structure with multi-scale conductive pathways. It demonstrates superior macroscopic electronic conductivity, along with electron transfer between the conductive polymer and CNTs. Therefore, the binder framework more effectively constrains the bulk expansion and void cracking of electrodes, while preventing derivatization reactions caused by continuous contact between the electrolyte and the anode particles and CNTs, thereby avoiding constant SEI growth. The stability of the bulk/interphase-structure (induced by only 5wt % novel binder without other additives) enables the commercial Gr/SiOx electrodes to exhibit significantly enhanced cycling performance and rate capability. The innovative binder design that effectively integrates conductivity, adhesion and mechanical strength offers new avenues for the large-scale application of high-performance electrodes with high anode material content.

#### Data availability

The data supporting the findings of this study are included within the article and Supplementary Information files.

#### CRediT authorship contribution statement

Lu Wang: Writing – review & editing, Writing – original draft, Visualization, Validation, Software, Methodology, Investigation, Formal analysis, Data curation, Conceptualization. Yan Zhao: Writing – review & editing, Supervision, Resources, Project administration, Methodology, Investigation, Funding acquisition, Formal analysis, Conceptualization. Hao Zhang: Methodology, Investigation, Data curation. Haoliang Wang: Methodology, Data curation. Chuanxi Chen: Data curation. Yuxiang Huang: Data curation. Haoyu Xue: Data curation. Yumeng Lan: Data curation. Fen Qiao: Data curation. Junfeng Wang: Data curation. Zirui Lou: Writing – review & editing, Supervision, Resources, Project administration, Methodology, Investigation, Funding acquisition, Formal analysis, Data curation. Feng Pan: Writing – review & editing, Supervision, Resources, Project administration, Methodology, Formal analysis, Data curation.

### Declaration of competing interest

The authors declare that they have no known competing financial interests or personal relationships that could have appeared to influence the work reported in this paper.

#### Acknowledgements

Y.Z. acknowledges financial support from Research Foundation for Advanced Talents of Jiangsu University, China (Grant No. 23JDG041). F.P. and Z.L. acknowledge financial support from the National Natural Science Foundation of China (No. 92472206), International joint Research Center for Electric Vehicle Power Battery and Materials (No. 2015B01015), Guangdong Key Laboratory of Design and calculation of

New Energy Materials (No. 2017B030301013), Shenzhen Key Laboratory of New Energy Resources Genome Preparation and Testing (No. ZDSYS201707281026184). We thank Prof. Xiaomin Xu from Tsinghua University for helpful technical support.

#### Supplementary materials

Supplementary material associated with this article can be found, in the online version, at doi:10.1016/j.ensm.2025.104255.

#### References

- [1] G.G. Eshetu, H. Zhang, X. Judez, H. Adenusi, M. Armand, S. Passerini, E. Figgemeier, Production of high-energy Li-ion batteries comprising siliconcontaining anodes and insertion-type cathodes, Nat. Commun. 12 (2021) 5459, https://doi.org/10.1038/s41467-021-25334-8.
- [2] G. Zhu, D. Chao, W. Xu, M. Wu, H. Zhang, Microscale silicon-based anodes: fundamental understanding and industrial prospects for practical high-energy lithium-ion batteries, ACS. Nano 15 (2021) 15567–15593, https://doi.org/ 10.1021/acsnapo.1005898.
- [3] M. Ge, C. Cao, G.M. Biesold, C.D. Sewell, S.-M. Hao, J. Huang, W. Zhang, Y. Lai, Z. Lin, Recent advances in silicon-based electrodes: from fundamental research toward practical applications, Adv. Mater. 33 (2021) 2004577, https://doi.org/ 10.1002/adma.202004577.
- [4] Z. Li, M. Du, X. Guo, D. Zhang, Q. Wang, H. Sun, B. Wang, Y.A. Wu, Research progress of SiOx-based anode materials for lithium-ion batteries, Chem. Eng. J. 473 (2023) 145294, https://doi.org/10.1016/j.cej.2023.145294.
- [5] M. Ashuri, Q. He, L.L. Shaw, Silicon oxides for Li-ion battery anode applications: toward long-term cycling stability, J. Power. Sources. 559 (2023) 232660, https://doi.org/10.1016/j.jpowsour.2023.232660.
- [6] S. Chen, Z. Song, L. Wang, H. Chen, S. Zhang, F. Pan, L. Yang, Establishing a resilient conductive binding network for Si-based anodes via Molecular engineering, Acc. Chem. Res. 55 (2022) 2088–2102, https://doi.org/10.1021/acs. accounts.200259.
- [7] Z. Song, L. Wang, K. Yang, Y. Gong, L. Yang, X. Liu, F. Pan, Intermolecular chemistry for designing functional binders in silicon/carbon composite anodes, Mater. Today Energy 30 (2022) 101153, https://doi.org/10.1016/j. mtener.2022.101153.
- [8] Y.-M. Zhao, F.-S. Yue, S.-C. Li, Y. Zhang, Z.-R. Tian, Q. Xu, S. Xin, Y.-G. Guo, Advances of polymer binders for silicon-based anodes in high energy density lithium-ion batteries, InfoMat 3 (2021) 460–501, https://doi.org/10.1002/ inf2.12185.
- [9] G. Qian, Y. Li, H. Chen, L. Xie, T. Liu, N. Yang, Y. Song, C. Lin, J. Cheng, N. Nakashima, M. Zhang, Z. Li, W. Zhao, X. Yang, H. Lin, X. Lu, L. Yang, H. Li, K. Amine, L. Chen, F. Pan, Revealing the aging process of solid electrolyte interphase on SiOx anode, Nat. Commun. 14 (2023) 6048, https://doi.org/ 10.1038/s41467-023-41867-6.
- [10] Z. He, C. Zhang, Z. Zhu, Y. Yu, C. Zheng, F. Wei, Advances in carbon nanotubes and carbon coatings as conductive networks in silicon-based anodes, Adv. Funct. Mater. 34 (2024) 2408285, https://doi.org/10.1002/adfm.202408285.
- [11] H. Wang, Y. Chao, J. Li, Q. Qi, J. Lu, P. Yan, Y. Nie, L. Wang, J. Chen, X. Cui, What is the real origin of single-walled carbon nanotubes for the performance enhancement of Si-based anodes? J. Am. Chem. Soc. 146 (2024) 17041–17053, https://doi.org/10.1021/jacs.4c01677.
- [12] B. Zhang, Y. Dong, J. Han, Y. Zhen, C. Hu, D. Liu, Physicochemical dual cross-linking conductive polymeric networks combining high strength and high toughness enable stable operation of silicon microparticle anodes, Adv. Mater. 35 (2023) 2301320, https://doi.org/10.1002/adma.202301320.
- [13] F. Zhang, H. Xia, T. Wei, H. Li, M. Yang, A.-M. Cao, A new universal aqueous conductive binder via esterification reinforced electrostatic/H-bonded selfassembly for high areal capacity and stable lithium-ion batteries, Energy Environ. Sci. 17 (2024) 238–248. https://doi.org/10.1039/D3FF02377.1.
- [14] Z. Song, T. Zhang, L. Wang, Y. Zhao, Z. Li, M. Zhang, K. Wang, S. Xue, J. Fang, Y. Ji, F. Pan, L. Yang, Bio-inspired binder design for a robust conductive network in silicon-based anodes, Small. Methods 6 (2022) 2101591, https://doi.org/10.1002/smtd.202101591.
- [15] Z. Song, S. Chen, Y. Zhao, S. Xue, G. Qian, J. Fang, T. Zhang, C. Long, L. Yang, F. Pan, Constructing a resilient hierarchical conductive network to promote cycling stability of SiO anode via binder design, Small. 17 (2021) 2102256, https://doi.org/10.1002/smll.202102256.
- [16] Y. Zhao, L. Yang, Y. Zuo, Z. Song, F. Liu, K. Li, F. Pan, Conductive binder for Si anode with boosted charge transfer capability via n-type doping, ACS. Appl. Mater. Interfaces. 10 (2018) 27795–27800, https://doi.org/10.1021/acsami.8b08843.
- [17] Y. Zhao, L. Yang, D. Liu, J. Hu, L. Han, Z. Wang, F. Pan, A conductive binder for high-performance Sn electrodes in lithium-ion batteries, ACS. Appl. Mater. Interfaces. 10 (2018) 1672–1677, https://doi.org/10.1021/acsami.7b13692.
- [18] D. Liu, Y. Zhao, R. Tan, L.-L. Tian, Y. Liu, H. Chen, F. Pan, Novel conductive binder for high-performance silicon anodes in lithium ion batteries, Nano Energy 36 (2017) 206–212, https://doi.org/10.1016/j.nanoen.2017.04.043.
- [19] H.A. Hoang, D. Kim, High energy and sustainable solid-state lithium-sulfur battery enabled by the force-bearing cathode and multifunctional double-layer hybrid

- solid electrolyte, Chem. Eng. J. 474 (2023) 145982, https://doi.org/10.1016/j.
- [20] T. Solomun, A. Schimanski, H. Sturm, E. Illenberger, Reactions of amide group with fluorine as revealed with surface analytics, Chem. Phys. Lett. 387 (2004) 312–316, https://doi.org/10.1016/j.cplett.2004.01.125.
- [21] A. Siriviriyanun, T. Imae, Advantages of immobilization of Pt nanoparticles protected by dendrimers on multiwalled carbon nanotubes, Phys. Chem. Chem. Phys. 14 (2012) 10622–10630, https://doi.org/10.1039/C2CP41364G.
- [22] L. Xiong, X. Fu, Y. Zhou, P. Nian, Z. Wang, Q. Yue, Precise site-hydrophobicity modulation for boosting high-performance CO2 electroreduction, ACS. Catal. 13 (2023) 6652–6660, https://doi.org/10.1021/acscatal.2c06106.
- [23] W. Zhang, Y.-W. Wang, R. Hu, L.-M. Fu, X.-C. Ai, J.-P. Zhang, J.-H. Hou, Mechanism of primary charge photogeneration in polyfluorene copolymer/ fullerene blends and influence of the donor/acceptor lowest unoccupied molecular orbital level offset, J. Phys. Chem. C 117 (2013) 735–749, https://doi.org/ 10.1021/jp308442t.
- [24] N.F. Hartmann, R. Pramanik, A.-M. Dowgiallo, R. Ihly, J.L. Blackburn, S.K. Doorn, Photoluminescence imaging of polyfluorene surface structures on semiconducting carbon nanotubes: implications for thin film exciton transport, ACS. Nano 10 (2016) 11449–11458, https://doi.org/10.1021/acsnano.6b07168.
- [25] C. Sun, H. Zhang, P. Mu, G. Wang, C. Luo, X. Zhang, C. Gao, X. Zhou, G. Cui, Covalently cross-linked chemistry of a three-dimensional network binder at limited dosage enables practical Si/C composite electrode applications, ACS. Nano 18 (2024) 2475–2484, https://doi.org/10.1021/acsnano.3c11286.
- [26] M. Xu, X. Wei, Z. Yan, J. Huang, S. Wu, K.-H. Ye, Z. Lin, A fast self-healing binder for highly stable SiOx anodes in lithium-ion batteries, ACS. Appl. Mater. Interfaces. 16 (2024) 55353–55361, https://doi.org/10.1021/acsami.4c11153.
- [27] G. Wu, Y. Gao, Z. Weng, Z. Zheng, W. Fan, A. Pan, N. Zhang, X. Liu, R. Ma, G. Chen, Binder-induced inorganic-rich solid electrolyte interphase and physicochemical dual cross-linked network for high-performance SiO anode, Carbon Neutralizat. 3 (2024) 857–872, https://doi.org/10.1002/cnl2.158.
- [28] Y. Kang, N. Dong, F. Liu, D. Lin, B. Liu, G. Tian, S. Qi, D. Wu, Constructing high-toughness polyimide binder with robust polarity and ion-conductive mechanisms ensuring long-term operational stability of silicon-based anodes, J. Energy Chem. 93 (2024) 580–591, https://doi.org/10.1016/j.jechem.2024.02.031.
- [29] Z. Liu, Y. Yang, Q. Zhu, M. Li, B. Xu, Enhanced lithium-ion storage of the SiOx@C anode enabled by carbon coating coupled with MXene as a conductive binder, Inorg. Chem. Front. 11 (2024) 1511–1521, https://doi.org/10.1039/D3Q102596A.
- [30] X. Yu, J. Liu, J. Wu, S. Ma, Y. Luo, X. Gao, Three-dimensional dual-layered conductive binder enables stable and high performance of SiOx/C anodes, J. Energy Storage 80 (2024) 110379, https://doi.org/10.1016/j.est.2023.110379.
- [31] H. Liu, J. Cai, P. Zhou, L. Li, Z. Ma, X. Zhao, J. Nan, A biomimetic green binder: forming a biomorphic polymer network in SiOx anode to buffer expansion and enhance performance, Chem. Eng. J. 475 (2023) 146284, https://doi.org/ 10.1016/j.cej.2023.146284.
- [32] Z. Weng, G. Wu, J. Li, Y. Zhang, R. Zhang, N. Zhang, X. Liu, C. Jia, G. Chen, Sulfonic group modified binder endows rapid lithium-ion diffusion for SiO microparticle anode, Small. Sci. 4 (2024) 2300133, https://doi.org/10.1002/ smsc.202300133.
- [33] Q. Zhang, J. Zhu, Y. Nie, S. Li, D. Wang, Y. Han, H. Wang, Y. Tian, Y. Han, X. Cui, Q. Xu, Hierarchical carbon nanofibers-based ternary conductive network built for improving electrochemical performance of SiOx@C anodes, Mater. Chem. Phys. 309 (2023) 128431, https://doi.org/10.1016/j.matchemphys.2023.128431.
  [34] J. Long, W. He, H. Liao, W. Ye, H. Dou, X. Zhang, In situ prepared three-
- [34] J. Long, W. He, H. Liao, W. Ye, H. Dou, X. Zhang, In situ prepared three-dimensional covalent and hydrogen bond synergistic binder to boost the performance of SiOx anodes for lithium-ion batteries, ACS. Appl. Mater. Interfaces. 15 (2023) 10726–10734, https://doi.org/10.1021/acsami.2c21689.
- [35] G. Wu, Z. Weng, J. Li, Z. Zheng, Z. Wen, W. Fang, Y. Zhang, N. Zhang, G. Chen, X. Liu, Body armor-inspired double-wrapped binder with high energy dispersion for a stable SiOx anode, ACS. Appl. Mater. Interfaces. 15 (2023) 34852–34861, https://doi.org/10.1021/acsami.3c05228.
- [36] J. Li, K. Yang, Y. Zheng, S. Gao, J. Chai, X. Lei, Z. Zhan, Y. Xu, M. Chen, Z. Liu, Q. Guo, Water-soluble polyamide acid binder with fast Li+ transfer kinetics for silicon suboxide anodes in lithium-ion batteries, ACS. Appl. Mater. Interfaces. 15 (2023) 30302–30311, https://doi.org/10.1021/acsami.3c05103.
- [37] S. Kim, D.-Y. Han, G. Song, J. Lee, T. Park, S. Park, Resilient binder network with enhanced ionic conductivity for high-areal-capacity Si-based anodes in Lithium-Ion batteries, Chem. Eng. J. 473 (2023) 145441, https://doi.org/10.1016/j. cai.2023.145441
- [38] C. Gao, H. Zhang, P. Mu, R. Wu, X. Zhang, X. Chen, C. Sun, Q. Wang, G. Cui, Hard–Soft segment synergism binder facilitates the implementation of practical SiC600 electrodes, Adv. Energy Mater. 13 (2023) 2302411, https://doi.org/ 10.1002/aenm.202302411.
- [39] D.-Y. Han, I.K. Han, H. Bin Son, Y.S. Kim, J. Ryu, S. Park, Layering charged polymers enable highly integrated high-capacity battery anodes, Adv. Funct. Mater. 33 (2023) 2213458, https://doi.org/10.1002/adfm.202213458.
- [40] S. Di, D. Zhang, Z. Weng, L. Chen, Y. Zhang, N. Zhang, R. Ma, G. Chen, X. Liu, Crosslinked polymer binder via phthalic acid for stabilizing SiO anodes, Macromol. Chem. Phys. 223 (2022) 2200068, https://doi.org/10.1002/macp.202200068.
- [41] H. Xiao, J. Qiu, S. Wu, L. Xie, W. Zhou, X. Wei, K.N. Hui, M. Zhang, Z. Lin, Cross-linked γ-polyglutamic acid as an aqueous SiOx anode binder for long-term lithium-ion batteries, ACS. Appl. Mater. Interfaces. 14 (2022) 18625–18633, https://doi.org/10.1021/accspni.2003458
- [42] Z. Li, W. Tang, Y. Yang, G. Lai, Z. Lin, H. Xiao, J. Qiu, X. Wei, S. Wu, Z. Lin, Engineering prelithiation of polyacrylic acid binder: a universal strategy to boost

- initial coulombic efficiency for high-areal-capacity Si-based anodes, Adv. Funct. Mater. 32 (2022) 2206615, https://doi.org/10.1002/adfm.202206615.
- [43] Z. Weng, S. Di, L. Chen, G. Wu, Y. Zhang, C. Jia, N. Zhang, X. Liu, G. Chen, Random copolymer hydrogel as elastic binder for the SiOx microparticle anode in lithium-ion batteries, ACS. Appl. Mater. Interfaces. 14 (2022) 42494–42503, https://doi.org/10.1021/acsami.2c12128.
- [44] T. Zhu, T.-N. Tran, C. Fang, D. Liu, S.P. Herle, J. Guan, G. Gopal, A. Joshi, J. Cushing, A.M. Minor, G. Liu, Lithium substituted poly(amic acid) as a watersoluble anode binder for high-temperature pre-lithiation, J. Power. Sources. 521 (2022) 230889, https://doi.org/10.1016/j.jpowsour.2021.230889.
- [45] Y. Li, B. Jin, K. Wang, L. Song, L. Ren, Y. Hou, X. Gao, X. Zhan, Q. Zhang, Coordinatively-intertwined dual anionic polysaccharides as binder with 3D network conducive for stable SEI formation in advanced silicon-based anodes, Chem. Eng. J. 429 (2022) 132235, https://doi.org/10.1016/j.cej.2021.132235.
- [46] W. Tang, L. Feng, X. Wei, G. Lai, H. Chen, Z. Li, X. Huang, S. Wu, Z. Lin, Three-dimensional crosslinked PAA-TA hybrid binders for long-cycle-life SiOx anodes in lithium-ion batteries, ACS. Appl. Mater. Interfaces. 14 (2022) 56910–56918, https://doi.org/10.1021/acsami.2c19344.
- [47] Z. Wang, X. Xu, C. Chen, T. Huang, A. Yu, Natural sesbania gum as an efficient biopolymer binder for high-performance Si-based anodes in lithium-ion batteries, J. Power. Sources. 539 (2022) 231604, https://doi.org/10.1016/j. ipowsour.2022.231604.
- [48] H. Liao, N. Liu, W. He, J. Long, H. Dou, X. Zhang, Three-dimensional cross-linked binder based on ionic bonding for a high-performance SiOx anode in lithium-ion batteries, ACS. Appl. Energy Mater. 5 (2022) 4788–4795, https://doi.org/ 10.1021/acsaem.2c00221.
- [49] H. Liu, E. Huangzhang, C. Sun, Y. Fan, Z. Ma, X. Zhao, J. Nan, SiOx/C composite anode of lithium-ion batteries with enhanced performances using multicomponent binders, ACS. Omega 6 (2021) 26805–26813, https://doi.org/10.1021/ acsomega.1c04544.
- [50] H. Liao, W. He, N. Liu, D. Luo, H. Dou, X. Zhang, Facile In situ cross-linked robust three-dimensional binder for high-performance SiOx anodes in lithium-ion batteries, ACS. Appl. Mater. Interfaces. 13 (2021) 49313–49321, https://doi.org/ 10.1021/acsami.1c13937.
- [51] S. Wu, Y. Yang, C. Liu, T. Liu, Y. Zhang, B. Zhang, D. Luo, F. Pan, Z. Lin, In-situ polymerized binder: a three-in-one design strategy for all-integrated SiOx anode with high mass loading in lithium ion batteries, ACS. Energy Lett. 6 (2021) 290–297
- [52] D. He, P. Li, W. Wang, Q. Wan, J. Zhang, K. Xi, X. Ma, Z. Liu, L. Zhang, X. Qu, Collaborative design of hollow nanocubes, In situ cross-linked binder, and amorphous Void@SiO@C as a three-pronged strategy for ultrastable lithium storage, Small. 16 (2020) 1905736. https://doi.org/10.1002/smll.201905736.
- [53] C. Zhang, Q. Chen, X. Ai, X. Li, Q. Xie, Y. Cheng, H. Kong, W. Xu, L. Wang, M.-S. Wang, H. Yang, D.-L. Peng, Conductive polyaniline doped with phytic acid as a binder and conductive additive for a commercial silicon anode with enhanced lithium storage properties, J. Mater. Chem. A Mater. 8 (2020) 16323–16331, https://doi.org/10.1039/D0TA04389C.
- [54] C. Luo, X. Wu, T. Zhang, S.-S. Chi, Z. Liu, J. Wang, C. Wang, Y. Deng, A four-armed polyacrylic acid homopolymer binder with enhanced performance for SiO/graphite anode, Macromol. Mater. Eng. 306 (2021) 2000525, https://doi.org/10.1002/ mame. 202000525
- [55] T. Zhao, Y. Meng, H. Yin, K. Guo, R. Ji, G. Zhang, Y. Zhang, Beneficial effect of green water-soluble binders on SiOx/graphite anode for lithium-ion batteries, Chem. Phys. Lett. 742 (2020) 137145, https://doi.org/10.1016/j. cplett.2020.137145.
- [56] Y. Cho, J. Kim, A. Elabd, S. Choi, K. Park, T. Kwon, J. Lee, K. Char, A. Coskun, J. W. Choi, A pyrene–Poly(acrylic acid)–Polyrotaxane supramolecular binder network for high-performance silicon negative electrodes, Advanced Materials 31 (2019) 1905048, https://doi.org/10.1002/adma.201905048.
- [57] T. Kang, J. Chen, Y. Cui, Z. Wang, H. Xu, Z. Ma, X. Zuo, X. Xiao, J. Nan, Three-dimensional rigidity-reinforced SiOx anodes with stabilized performance using an aqueous multicomponent binder technology, ACS. Appl. Mater. Interfaces. 11 (2019) 26038–26046, https://doi.org/10.1021/acsami.9b08389.
- [58] K. Yang, Z. Yu, C. Yu, M. Zhu, L. Yang, H. Chen, F. Pan, A. Versatile, Polymeric precursor to high-performance silicon composite anode for lithium-ion batteries, Energy Technol. 7 (2019) 1900239, https://doi.org/10.1002/ente.201900239.
- [59] Z. He, C. Zhang, Y. Zhu, F. Wei, The acupuncture effect of carbon nanotubes induced by the volume expansion of silicon-based anodes, Energy Environ. Sci. 17 (2024) 3358–3364, https://doi.org/10.1039/D4EE00710G.
- [60] Y. Huang, Y. Ji, G. Zheng, H. Cao, H. Xue, X. Yao, L. Wang, S. Chen, Z. Yin, F. Pan, L. Yang, Tailored interphases construction for enhanced Si anode and Ni-rich cathode performance in lithium-ion batteries, CCS Chem. 0 (n.d.) 1–11. https://doi.org/10.31635/ccschem.024.202404120.
- [61] T. Hou, G. Yang, N.N. Rajput, J. Self, S.-W. Park, J. Nanda, K.A. Persson, The influence of FEC on the solvation structure and reduction reaction of LiPF6/EC electrolytes and its implication for solid electrolyte interphase formation, Nano Energy 64 (2019) 103881, https://doi.org/10.1016/j.nanoen.2019.103881.
- [62] A. Huang, Z. Ma, P. Kumar, H. Liang, T. Cai, F. Zhao, Z. Cao, L. Cavallo, Q. Li, J. Ming, Low-temperature and fast-charging lithium metal batteries enabled by Solvent–Solvent interaction mediated electrolyte, Nano Lett. 24 (2024) 7499–7507, https://doi.org/10.1021/acs.nanolett.4c01591.
- [63] A.L. Michan, B.S. Parimalam, M. Leskes, R.N. Kerber, T. Yoon, C.P. Grey, B. L. Lucht, Fluoroethylene carbonate and vinylene carbonate reduction: understanding lithium-ion battery electrolyte additives and solid electrolyte interphase formation, Chem. Mater. 28 (2016) 8149–8159, https://doi.org/10.1021/acs.chemmater.6b02282.

- [64] Y. Yang, J. Wang, Z. Li, Z. Yang, B. Wang, H. Zhao, Constructing LiF-dominated interphases with polymer interwoven outer layer enables long-term cycling of Si anodes, ACS. Nano 18 (2024) 7666–7676, https://doi.org/10.1021/ acspano 4c00998
- [65] A. Wang, S. Kadam, H. Li, S. Shi, Y. Qi, Review on modeling of the anode solid electrolyte interphase (SEI) for lithium-ion batteries, NPJ. Comput. Mater. 4 (2018) 15, https://doi.org/10.1038/s41524-018-0064-0.
- [66] J. Tan, J. Matz, P. Dong, J. Shen, M. Ye, A growing appreciation for the role of LiF in the solid electrolyte interphase, Adv. Energy Mater. 11 (2021) 2100046, https://doi.org/10.1002/aepm.202100046
- doi.org/10.1002/aenm.202100046.
  [67] J. Chen, X. Fan, Q. Li, H. Yang, M.R. Khoshi, Y. Xu, S. Hwang, L. Chen, X. Ji, C. Yang, H. He, C. Wang, E. Garfunkel, D. Su, O. Borodin, C. Wang, Electrolyte design for LiF-rich solid–electrolyte interfaces to enable high-performance microsized alloy anodes for batteries, Nat. Energy 5 (2020) 386–397, https://doi.org/10.1038/s41560-020-0601-1.